Determination of the Rate Constant of the [4 + 2] Cycloaddition Between an Aryne Atropisomer and Furan in Solution

Guillaume Dauvergne, Nicolas Vanthuyne, Michel Giorgi, Jean Rodriguez, Yannick Carissan, Yoann Coquerel

▶ **To cite this version:**

Guillaume Dauvergne, Nicolas Vanthuyne, Michel Giorgi, Jean Rodriguez, Yannick Carissan, et al.. Determination of the Rate Constant of the [4 + 2] Cycloaddition Between an Aryne Atropisomer and Furan in Solution. Journal of Organic Chemistry, 2022, 87 (16), pp.11141-11147. 10.1021/acs.joc.2c01394 . hal-03777717

HAL Id: hal-03777717
https://hal.science/hal-03777717

Submitted on 15 Sep 2022

HAL is a multi-disciplinary open access archive for the deposit and dissemination of scientific research documents, whether they are published or not. The documents may come from teaching and research institutions in France or abroad, or from public or private research centers.

L'archive ouverte pluridisciplinaire **HAL**, est destinée au dépôt et à la diffusion de documents scientifiques de niveau recherche, publiés ou non, émanant des établissements d'enseignement et de recherche français ou étrangers, des laboratoires publics ou privés.

Determination of the Rate Constant of the [4 + 2] Cycloaddition Between an Aryne Atropisomer and Furan in Solution

Guillaume Dauvergne, Nicolas Vanthuyne, Michel Giorgi, Jean Rodriguez, Yannick Carissan,* and Yoann Coquerel*

ABSTRACT: Using a specially designed prototype of a nonracemic aryne atropisomer with a low barrier to enantiomerization (*ca.* 36 kJ·mol^{-1}), it was possible to determine the kinetic constant of its cycloaddition with furan in solution by a combination of theoretical calculations and experimental measurements. It was found that the reaction half-life of this aryne atropisomer in solution with 100 equivalents of furan as the trapping reagent is <150 ns at temperatures above −20 °C.

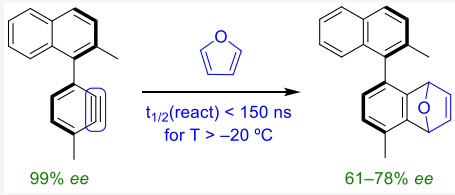

INTRODUCTION

ortho-Arynes, or simply arynes, are now established as versatile tools in synthetic organic chemistry with a variety of applications for the synthesis of partially or fully aromatic molecules, from complex natural products to large polycyclic aromatic hydrocarbons.[1] Arynes are electrophilic species that generally react with nucleophiles in addition reactions, and with unsaturated molecules in cycloaddition reactions. Theoretical analyses of the electronic structure and aromaticity of arynes using magnetic criteria showed that arynes are aromatic species and are better described as acetylene-containing rather than cumulene-containing molecules.[2] But it should be kept in mind that the traditional Lewis structure of arynes with a triple bond is an oversimplification. Indeed, the two-electron reacting π system in arynes is composed of two weakly overlapping sp^2-resembling orbitals, which is, in part, responsible for the high chemical reactivity of arynes. Arynes are notoriously short-lived species that must be generated *in situ*, most commonly through the ortho-elimination of a suitable aromatic precursor.[3] But how long do arynes really live in solution?

The first kinetic data on benzyne were provided in 1964 by Ebel and Hoffmann who generated gaseous benzyne by thermolysis of *bis*(2-iodophenyl)mercury, which was trapped downstream by vapors of furan.[4] Subsequently, follow-ups on the gas-phase dimerization of benzyne into biphenylene were performed. Schafer and Berry examined this reaction by vacuum flash photolysis of benzenediazonium 2-carboxylate to generate benzyne, and using time-resolved optical and mass spectroscopy, they determined that the second order rate constant for benzyne dimerization k_{dimer} is at least equal to 8.0×10^8 L·mol^{-1}·s^{-1}.[5] These results were completed by Porter and Steinfeld who generated gaseous benzyne by vacuum flash photolysis of phthalic anhydride and measured the rate constant k_{dimer} at 4.6×10^9 L·mol^{-1}·s^{-1}.[6] More recently, femtosecond time-resolved mass spectrometry allowed the observation of gaseous benzyne generated from 1,2-dibromobenzene in a molecular beam and revealed a lifetime of 400 ps or more before Bergman rearrangement.[7] However, no experimental data exist about the kinetics of arynes in solution.

To gain knowledge about the lifetime of arynes in solution, computational modeling has proven useful, especially using DFT methods. For instance, the barrier to the reaction between benzyne and furan was recently computed at $\Delta G^{\ddagger}_{react}$ = 32.6 kJ·mol^{-1} at 25 °C using the SMD(acetonitrile)/B3LYP-D3BJ/6-311+G(d,p)//B3LYP/6-31G(d) level of theory.[8] Our own calculations for the same reaction at the SMD(diethyl ether)/M062X-D3/aug-cc-pVDZ//M062X-D3/cc-pVDZ level of theory afforded $\Delta G^{\ddagger}_{react}$ = 36.4 kJ·mol^{-1} at 25 °C (see Supporting Information, Figure S1). In the hypothesis of first-order reactions, these values of $\Delta G^{\ddagger}_{react}$ correspond to half-lives of 57 and 266 ns, respectively, for benzyne.

The enantiospecific generation and trapping reactions of nonracemic aryne atropisomers based on a 1-phenylnaphthalene backbone were reported recently (Scheme 1a).[9] In these cases, the rates of reaction of the aryne atropisomers are greater than their rates of enantiomerization by several orders of magnitude, which allowed for highly enantiospecific reactions. For the present work, it was devised that the generation and trapping reaction of a specially designed aryne atropisomer having a barrier to enantiomerization in the magnitude of its barrier to reaction would allow for measuring experimentally some meaningful variations of the enantiospecificity during its

Scheme 1. Aryne Atropisomers With a 1-Phenylnaphthalene Backbone; (a) Conformationally Stable Aryne Atropisomers (ref 9); (b) Conformationally Labile Aryne Atropisomer

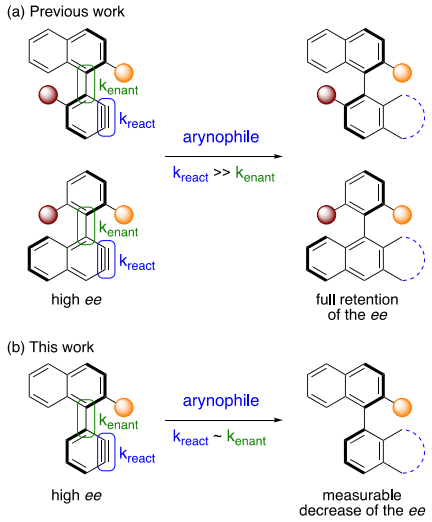

reactions (Scheme 1b). Based on the accurate calculation of the barrier to enantiomerization of such an aryne atropisomer, it should thus be possible to determine the kinetic constants of its [4 + 2] cycloadditions with furan.

RESULTS AND DISCUSSION

The enantiomerization barriers of several aryne atropisomers were previously evaluated by computational DFT methods, typically B3LYP-D3/6-311++G(d,p).[9] It was identified that the barriers to enantiomerization of aryne atropisomers are significantly lower than the barriers to enantiomerization of the corresponding biaryl derivatives having two C(sp^2)−H bonds in place of the aryne triple bond due to a lack of repulsive van der Waals interactions with the H atom ortho to the stereogenic axes. The barrier to the reaction between benzyne and furan is computed at $\Delta G^{\ddagger}_{react}$ = 32.6−36.4 kJ·mol^{-1} by DFT methods, and it was searched *in silico* for a prototype of an aryne atropisomer with an enantiomerization barrier computed at $\Delta G^{\ddagger}_{enant}$ ~ 30−35 kJ·mol^{-1} by comparable methods. The aryne atropisomer **1** was identified as a suitable prototype (Figure 1), with a computed barrier to enantiomerization of $\Delta G^{\ddagger}_{enant}$ = 25.1−33.9 kJ·mol^{-1} at 25 °C depending on the DFT functional employed with the def2-TZVP basis set (see Supporting Information, Table S1). During the search for prototype **1**, the introduction of a methyl group ortho to the stereogenic axis on the naphthyl unit was found to be the best compromise between the high configurational stability of the precursor and the low configurational stability of the corresponding aryne atropisomer, both factors being crucial for the feasibility of the study. Aiming at more accurate values for the enantiomerization barrier of **1**, the electronic energies of the stationary points identified by DFT were recomputed at the CCSD(T*)-F12*/def2-TZVP level of theory,[10] and Gibbs free energies were obtained by applying the vibrational correction and solvation effects from the corresponding DFT calculations. The barrier to enantiomerization of aryne atropisomer **1** calculated this way is in the 34.3−38.7 kJ·mol^{-1} range at 25 °C with an average value of $\Delta G^{\ddagger}_{enant}$ = 36.3 kJ·mol^{-1} (Figure 1, see details in the Supporting Information, Table S2).

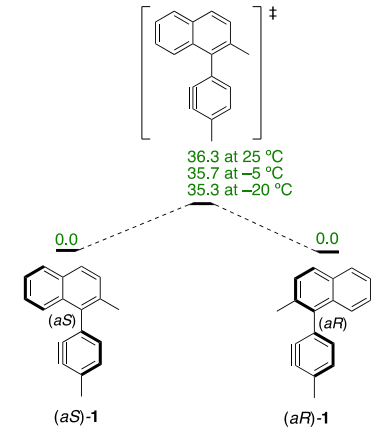

Figure 1. Enantiomerization barrier of aryne atropisomer **1** using the average of six CCSD(T*)-F12*//DFT calculations at 25, −5, and −20 °C. Values are Gibbs free energies expressed in kJ·mol^{-1}.

The average of the six values of $\Delta G^{\ddagger}_{enant}$ thus obtained was considered a good approximation of $\Delta G^{\ddagger}_{enant}$ of aryne atropisomer **1**. It may be noted that DFT methods somehow underestimate the enantiomerization barrier in this case.

To confront the refined CCSD(T*)-F12*//DFT computational model with an experimentally measured value and to verify that the computed $\Delta G^{\ddagger}_{enant}$ for aryne atropisomer **1** is reliable, the barrier to rotation of 1-(2′,6′-dideutero-4′-methylphenyl)naphthalene was calculated at a similar level of theory and found to agree well with its experimentally measured value at −28 °C:[11] $\Delta G^{\ddagger}_{rot}$ (exp.) = 48.6 ± 0.5 kJ·mol^{-1} *vs* $\Delta G^{\ddagger}_{rot}$ (calc.) = 49.7 kJ·mol^{-1} (<2.3% deviation, see details in the Supporting Information, Figure S2 and Table S3).

The [4 + 2] cycloaddition of aryne atropisomer **1** with furan should produce the diastereomeric cycloadducts **2a** and **2b** (Figure 2). Using the SMD(diethyl ether)/M062X-D3/aug-cc-pVDZ//M062X-D3/cc-pVDZ DFT model, the barrier to

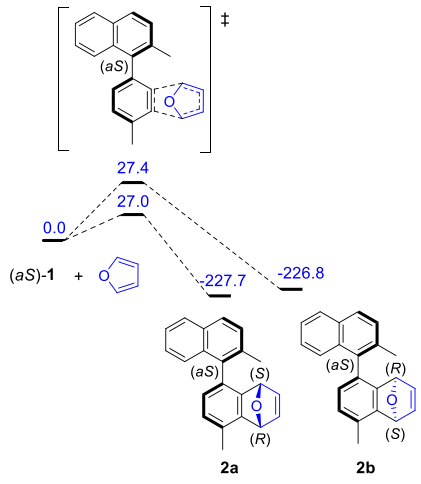

Figure 2. Energy profile of the reaction of aryne atropisomer **1** with furan. Values are Gibbs free energies expressed in kJ·mol^{-1} computed using DFT with SMD(diethyl ether)/M062X-D3/aug-cc-pVDZ//M062X-D3/cc-pVDZ at 25 °C.

reaction $\Delta G^{\ddagger}_{react}$ for these cycloadditions was computed at 27.0 and 27.4 kJ·mol^{-1} at 25 °C, indicating that aryne atropisomer **1** is more reactive than benzyne itself in the presence of furan in solution ($\Delta G^{\ddagger}_{react}$ = 36.4 kJ·mol^{-1} for benzyne at the same level of theory, see Figure S1). It was supposed that the nonracemic aryne atropisomer (*aS*)-**1** could be generated enantiospecifically from the nonracemic iodoaryl triflate precursor (*aS*)-**7** (Scheme 2).[9,12] The synthesis of (*aS*)-**7** was accomplished by a Suzuki

Scheme 2. Synthesis of the Aryne Atropisomer Precursor (*aS*)-7[a]

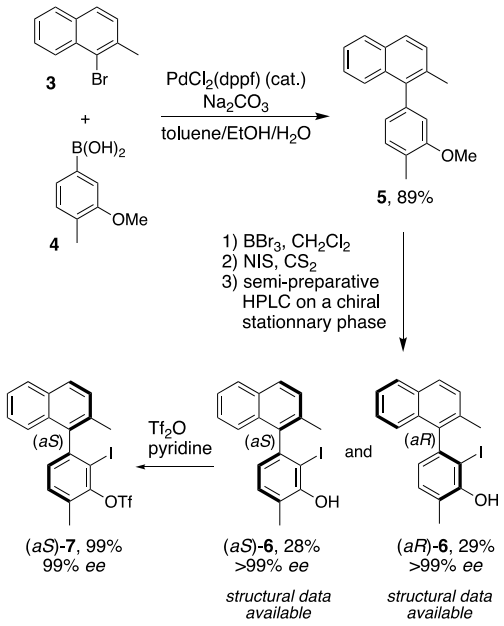

[a]NIS = *N*-iodosuccinimide

coupling between bromide **3** and boronic acid **4** for the construction of the biaryl axis in **5**, followed by deprotection to give intermediate **A** (not shown) and ortho-iodination to afford racemic **6**. The barrier to enantiomerization of **6** was estimated at 196.8 kJ·mol^{-1} by DFT methods (see Supporting Information, Figure S3), and the atropisomers of **6** could be resolved by semi-preparative HPLC methods to obtain enantiomerically pure materials. The structures and absolute configurations of both atropisomers (*aS*)-**6** and (*aR*)-**6** were secured by X-ray diffraction analyses of monocrystalline samples (see Supporting Information for details, Figures S4 and S5, and Table S4). Finally, triflation of (*aS*)-**6** afforded the expected iodoaryl triflate precursor (*aS*)-**7** with 99% *ee*.

The generation of aryne atropisomer (*aS*)-**1** from (*aS*)-7 was attempted at −5 and −20 °C in the presence of excess furan (100 equiv) so that its variation in concentration can be neglected (pseudo-first-order reaction, Scheme 3). At both temperatures, the expected cycloadduct was obtained as a 1:1 mixture of the two possible diastereomers **2a** and **2b** that are supposed to be configurationally stable under the conditions of the experiments and the analyses with $\Delta G^{\ddagger}_{enant}$ > 131 kJ·mol^{-1} at 25 °C determined by DFT calculations [SMD(diethyl ether)/M062X-D3/def2-SVP, see Supporting Information Figure S3]. The enantiomeric excesses of diastereomers **2a** and **2b** were measured at 66 and 61% for the reaction conducted at −5 °C, and at 78 and 76% for the reaction conducted at −20 °C, respectively. The measurable variations in the *ee* during the reaction show that the enantiomerization of the aryne atropisomer (*aS*)-**1** is kinetically competing with its [4 + 2] cycloaddition with furan. Considering that the reaction is occurring as depicted in Figure 2 and that the calculated barrier to enantiomerization of (*aS*)-**1** is accurate enough, it is possible to determine the rate of the cycloaddition between aryne atropisomer **1** and furan from the experimentally measured variations in *ee*. Calculation of the barriers to enantiomerization of (*aS*)-**1** using the average of six CCSD(T*)-F12*//DFT calculations at −5 and −20 °C gave $\Delta G^{\ddagger}_{enant}$ = 35.7 and 35.3 kJ·mol^{-1}, respectively (Figure 1). The rates of enantiomerization of (*aS*)-**1** at −5 and −20 °C were obtained from the Eyring equation as k_{enant}(−5 °C) = 0.61 × 10^{6} s^{-1} and k_{enant}(−20 °C) = 0.27 × 10^{6} s^{-1}. Using the difference of *ee* between the aryne atropisomer (*aS*)-**1** at the start and the cycloadducts **2a** and **2b** when the reaction is over, it is possible to determine the reaction time t_{max} in each of the four cases with t_{max}(−5 °C) = 330 and 394 ns, and t_{max}(−20 °C) = 440 and 488 ns (see Supporting

Scheme 3. [4 + 2] Cycloaddition of the Aryne Atropisomer (*aS*)-1 With Furan

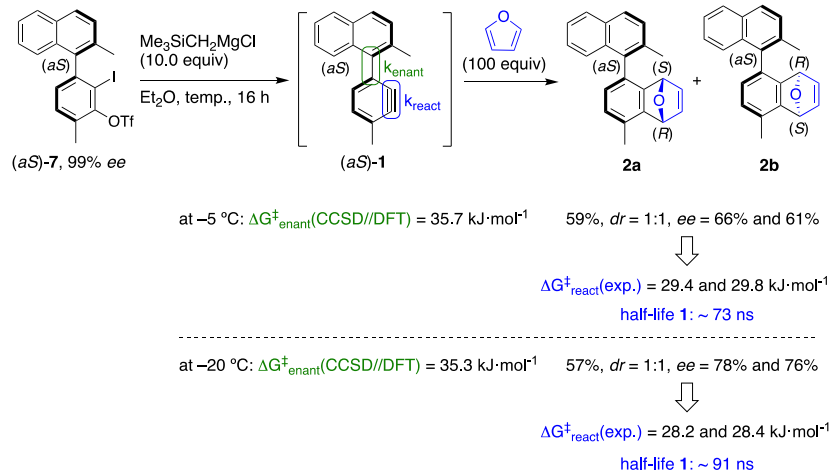

Information for the equations), respectively. Considering that $t_{max} \sim 5 \cdot t_{1/2}$, it is possible to determine the corresponding reaction rates $k_{react} = \ln 2/t_{1/2}$, which afforded $k_{react}(-5\ °C) = 10.5 \times 10^6$ and $8.8 \times 10^6\ s^{-1}$ and $k_{react}(-20\ °C) = 7.9 \times 10^6$ and $7.1 \times 10^6\ s^{-1}$, respectively. Using the Eyring equation, the four corresponding barriers to reaction could be determined as $\Delta G^{‡}_{react}(-5\ °C) = 29.4$ and 29.8 kJ·mol^{-1} and $\Delta G^{‡}_{react}(-20\ °C) = 28.2$ and 28.4 kJ·mol^{-1} for the formation of diastereomers **2a** and **2b**, respectively.

These values of $\Delta G^{‡}_{react}$ correspond to averaged reaction half-lives of 73 ns and 91 ns for the aryne atropisomer **1** at −5 and −20 °C, respectively. The reliability of the determined reaction half-lives of aryne atropisomer **1** is based on the accuracy of the calculation of its barrier to enantiomerization at −5 and −20 °C. A ±1 kJ·mol^{-1} deviation from the computed values of $\Delta G^{‡}_{enant}$ (2.8% deviation) would result in reaction half-lives of aryne atropisomer **1** to be in the 42−124 ns range at −5 °C, and the 54−153 ns range at −20 °C.

CONCLUSIONS

Using the specially designed nonracemic aryne atropisomer **1**, the kinetic constant of its cycloaddition with furan in solution could be determined by a combination of theoretical calculations and experimental measurements. The reaction half-life of this aryne atropisomer in solution with excess furan as the trapping reagent was determined to be <150 ns at temperatures above −20 °C. This study quantitatively demonstrates that the high reactivity of aryne atropisomers allows for enantiospecific trapping reactions, even for some fast-racemizing congeners, if their barrier to reaction is significantly lower than their barrier to enantiomerization.

EXPERIMENTAL SECTION

Calculations. The density functional theory (DFT) calculations reported in this section were performed with the Gaussian16 suite.[13] All geometries were fully optimized using either B3LYP,[14] M06, M062X,[15] MN15,[16] PBE0,[17] TPSSh, or[18] BP86[19] density functional with either 6-31G(d),[20] 6-311++G(d,p), cc-pVDZ,[21] aug-cc-pVDZ, cc-pVTZ, or def2-TZVP[22] basis set with pseudo potential correction[23] for I atoms in the gas phase or using the IEFPCM solvation model[24] or its SMD variation.[25] Calculations using the coupled cluster single and double (CCSD) level of theory including triple excitations (T*) and F12* correction in the gas phase were performed with the Turbomole v7.5 suite.[26] Dispersion effects were accounted for using Grimme's D3 dispersion model.[27] For all stationary points, the second derivatives were analytically calculated in order to determine if a minimum (zero negative eigenvalue) or a transition state (one negative eigenvalue) existed for this geometry. The connection between the transition states and the corresponding minima was performed manually by minimal steepest descend optimization. All energies are relative Gibbs free energies expressed in kJ·mol^{-1} as computed at 298 K unless otherwise stated.

*Barrier to Enantiomerization of the Aryne Atropisomer **1**.* Exploration of the potential energy surface for the aryne atropisomer **1** was performed with B3LYP/6-31G(d) level of theory in the gas phase. Two possible transition states corresponding to the rotation around the stereogenic axis could be located, **TS-enant-1#1** having the H atom of the naphthyl moiety overhanging the aryne being favored by 4.6 kJ·mol^{-1} over **TS-enant-1#2**. Then, the geometries of (*aS*)-**1** and **TS-enant-1#1** were optimized at the B3LYP-D3, M06-D3, M062X-D3, MN15, PBE0-D3, and TPPSh levels of theory with the def2-TZVP basis set including the IEFPCM solvation model for diethyl ether. The nature of each optimized structure was verified by frequency calculation at the same level of theory. Computed electronic and thermodynamic energies are summarized in Table S1 (see Supporting Information). Then, single-point calculations were carried out at the CCSD(T*)-F12*/def2-TZVP level of theory in the gas phase for each optimized geometry to give more accurate electronic energies ΔE_{elec}. The solvation correction ΔE_{solv} and the thermal correction to the Gibbs free energy ΔG_{corr} derived from the DFT calculations were then applied. These results are summarized in Table S2 (see Supporting Information).

Barrier to Rotation of 1-(2′,6′-dideutero-4′-methylphenyl)-naphthalene. Using the CCSD(T*)-F12*/def2-TZVP//PBE0-D3/def2-TZVP level of theory (best approximation as determined for **1**, see Table S2) with the SMD solvation model for the "*n*-methylformamide-mixture" to account for the oriented solvent used for the experimental measurements (liquid crystal made of poly-γ-benzyl-L-glutamate), the computed barrier to rotation of 1-(2′,6′-dideutero-4′-methylphenyl)-naphthalene was determined at $\Delta G^{‡}_{rot}$ (calc.) = 49.7 kJ·mol^{-1} (see Supporting Information, Table S3 and Figure S2).

*[4 + 2] Cycloaddition of the Aryne Atropisomer **1** and Benzyne with Furan Affording **2a** and **2b**.* The geometry of each stationary point was first optimized in the gas phase at the M062X-D3/cc-pVDZ level of theory. The nature of each stationary point was verified by frequency calculation. Single point calculations were then carried out at the M062X-D3/aug-cc-pVDZ level of theory using the SMD solvation model for diethyl ether (Figures 2 and S1).

*Configurational Stability of Atropisomers (aS)-**6**, (aS)-**2a**, and (aS)-**2b**.* Exploration of the potential energy surface for the conformations of (*aS*)-**6** was first performed at the BP86/cc-pVDZ level of theory set with pseudo potential correction for the I atom in the gas phase. Two possible transition states corresponding to the rotation around the stereogenic axis could be located, with **TS-enant-6#1** having the H atom of the naphthyl moiety overhanging the iodine atom being favored by 12.8 kJ·mol^{-1} over **TS-enant-6#2** (see Supporting Information, Figure S3). Next, the geometries and Gibbs free energies of the kinetically favored enantiomerization pathway were recomputed at the M062X-D3/def2-TZVP level of theory with pseudo potential correction for I atom including the IEFPCM solvation model for diethyl ether. For (*aS*)-**2a** and (*aS*)-**2b**, the exploration of the potential energy surface for the conformations was performed with M062X-D3/def2-SVP using the SMD solvation model for diethyl ether. The four possible transition states could be located, with **TS-enant-2a#1** being favored by 17.5 kJ·mol^{-1} over **TS-enant-2a#2**, and **TS-enant-2b#1** being favored by 17.5 kJ·mol^{-1} over **TS-enant-2b#2**.

Syntheses and Characterization. Reactions were carried out under an argon atmosphere in oven-dried reaction vessels in anhydrous organic solvents. All reagents were weighed and handled in air at room temperature unless otherwise mentioned, and all commercially available reagents were used as received. Anhydrous dichloromethane, diethyl ether, and toluene were dried by filtration over solid dehydrating agents using a commercial solvent purification system. Anhydrous carbon disulfide was obtained directly from commercial sources. Thin layer chromatography was carried out on Merck Kieselgel 60 F_{254} 0.2 mm plates. Visualization was accomplished using ultraviolet light (254 and/or 365 nm) and/or chemical staining with an ethanolic solution of para-anisaldehyde with sulphuric acid as appropriate. Purifications were routinely performed using flash chromatography columns packed with 40−63 μm silica gel.

Melting points were recorded using the Büchi Melting Point B-540 or B-545 apparatus.

NMR data were generally recorded at 298 ± 3 K in deuterated chloroform at 400 or 500 MHz using the residual chloroform signal for ^{1}H NMR (δ = 7.26 ppm) and the deuterated solvent signal for ^{13}C NMR (δ = 77.16 ppm) as internal standards. Chemical shifts (δ) are in ppm, coupling constants (J) are in Hertz (Hz), and the classical abbreviations are used to describe the signal multiplicities. ^{13}C DEPT135 experiments were systematically conducted to support assignments.

High-resolution mass spectra (HRMS) were recorded in triplicate at the Spectropole (http://fr-chimie.univ-amu.fr/spectropole//) on a Waters Synapt G2 HDMS apparatus using a positive electrospray (ESI) ionization source.

Optical Rotations were measured in $CHCl_3$ on an Anton Paar MCP 200 or Anton Paar MCP 100 Polarimeter at λ = 589 nm. $[\alpha]_D$ values are

reported at a given temperature (°C) in degree·cm^2·g^{-1} with concentrations reported in g/100 mL.

HPLC analyses for the determination of enantiomeric excess were performed on a Merck-Hitachi system equipped with Lux-Amylose-1 and Lux-Cellulose-3 analytical columns.

Single crystal X-ray diffraction analyses were performed on a Rigaku Oxford Diffraction SuperNova diffractometer. Data collection reduction and multiscan ABSPACK correction were performed with CrysAlisPro (Rigaku Oxford Diffraction). Using Olex2,[28] the structures were solved by intrinsic phasing methods, with SHELXT[29] and SHELXL[30] being used for full matrix least square refinement.

Compound ***5***. To a degassed suspension of 1-bromo-2-methylnaphthalene **3** (1.00 g, 4.52 mmol), 3-methoxy-4-methylphenylboronic acid **4** (901 mg, 5.42 mmol), and Na_2CO_3 (2.49 g, 2.35 mmol) in a mixture toluene/EtOH/H_2O (36:24:5 mL) was added $PdCl_2$(dppf) (165 mg, 5 mol %) under an inert atmosphere (glovebox). The resulting black suspension was stirred at reflux overnight using an oil bath. After cooling down to room temperature, the reaction mixture was filtered over celite to remove insoluble components. The resulting solution was diluted with EtOAc and washed twice with water and once with brine. The organic phase was dried over anhydrous Na_2SO_4, filtered, and concentrated under reduced pressure to afford the crude product. Purification by flash chromatography on silica gel eluted with 10:1 pentane/$CHCl_3$ afforded the pure product **5** (1.05 g, 89%) as a colorless oil. **TLC** (pentane/$CHCl_3$ = 10:1) R*f* = 0.50; **HRMS** (ESI+) *m*/*z*: calcd for $C_{19}H_{19}O^+$, $[M + H]^+$ 263.1430; found, 263.1430; **^{1}H NMR** (400 MHz, $CDCl_3$): δ 7.84 (d, *J* = 8.4 Hz, 1H), 7.78 (d, *J* = 8.6 Hz, 1H), 7.48 (d, *J* = 8.4 Hz, 1H), 7.42 (d, *J* = 8.7 Hz, 1H), 7.40 (ddd, *J* = 9.0, 6.9, 1.2 Hz, 1H), 7.33 (ddd, *J* = 9.0, 7.0, 1.5 Hz, 1H), 7.26 (d, *J* = 7.2 Hz, 1H), 6.78 (dd, *J* = 7.5, 1.5 Hz, 1H), 6.74 (d, *J* = 1.1 Hz, 1H), 3.80 (s, 3H), 2.34 (s, 3H), 2.28 (s, 3H); **^{13}C{^{1}H} NMR** (101 MHz, $CDCl_3$): δ 157.9 (C), 138.6 (C), 138.6 (C), 133.3 (C), 133.2 (C), 132.1 (C), 130.7 (CH), 128.7 (CH), 127.8 (CH), 127.2 (CH), 126.4 (CH), 125.9 (CH), 125.3 (C), 124.9 (CH), 122.1 (CH), 112.1 (CH), 55.5 (CH_3), 20.9 (CH_3), 16.2 (CH_3).

Atropisomer ***6*** *via Intermediate* ***A***. To a solution of **5** (155 mg, 0.59 mmol) in anhydrous dichloromethane (5 mL) was slowly (*ca.* over 10 min) added a solution of BBr_3 (1.0 M in dichloromethane, 0.89 mL, 0.89 mmol) at 0 °C. Then the mixture was warmed to room temperature and monitored by TLC until no starting material is detectable by TLC analysis (1 h). The reaction was hydrolyzed with a saturated $NaHCO_3$ aqueous solution and extracted with EtOAc. The organic phase was successively washed with water and brine, dried over anhydrous Na_2SO_4, and filtered. After concentration in vacuo, the residue was purified by flash column chromatography on silica gel (pentane/EtOAc = 10:1) to provide the demethylated compound **A** as a colorless oil (128 mg, 87%). **TLC** (pentane/EtOAc = 10:1) R*f* = 0.75; **HRMS** (ESI+) *m*/*z*: calcd for $C_{18}H_{17}O^+$, $[M + H]^+$ 249.1274; found, 249.1275; **^{1}H NMR** (400 MHz, $CDCl_3$): δ 7.83 (d, *J* = 8.2 Hz, 1H), 7.77 (d, *J* = 8.3 Hz, 1H), 7.47 (d, *J* = 8.7 Hz, 1H), 7.41 (d, *J* = 8.5 Hz, 1H), 7.40 (ddd, *J* = 8.4, 6.7, 1.2 Hz, 1H), 7.33 (ddd, *J* = 8.4, 7.0, 1.4 Hz, 1H), 7.24 (d, *J* = 7.5 Hz, 1H), 6.76 (dd, *J* = 7.5, 1.5 Hz, 1H), 6.68 (d, *J* = 1.5 Hz, 1H), 4.68 (s, 1H), 2.37 (s, 3H), 2.26 (s, 3H); **^{13}C{^{1}H} NMR** (101 MHz, $CDCl_3$): δ 153.8 (C), 139.0 (C), 137.9 (C), 133.2 (C), 133.1 (C), 132.1 (C), 131.2 (CH), 128.7 (CH), 127.8 (CH), 127.3 (CH), 126.3 (CH), 125.9 (CH), 124.9 (CH), 122.8 (CH), 122.5 (C), 116.8 (CH), 20.9 (CH_3), 15.7 (CH_3).

A degassed solution of **A** (222 mg, 0.89 mmol) in anhydrous CS_2 (10 mL) was protected from light using aluminum foil and cooled to 15 °C before the addition of *N*-iodosuccinimide (211 mg, 0.94 mmol). The mixture was warmed to room temperature (23−25 °C) and stirred until the starting material is no longer detectable by TLC analysis (2 days). The solvent was removed in vacuo, and the residue was poured into a saturated $NaHCO_3$ aqueous solution and extracted three times with EtOAc. The organic layer was washed twice with water and once with brine, dried over anhydrous Na_2SO_4, filtered, and concentrated under reduced pressure to afford the crude product. Purification by flash chromatography on silica gel eluted with pentane/EtOAc = 50:1 afforded racemic **6** (252 mg, 75%) as a colorless oil. **TLC** (pentane/EtOAc = 50:1) R*f* = 0.32; **HRMS** (ESI+) *m*/*z*: calcd for $C_{18}H_{19}NOI^+$, $[M + NH_4]^+$ 392.0506; found, 392.0506; **^{1}H NMR** (400 MHz, $CDCl_3$): δ 7.85 (d, *J* = 8.4 Hz, 1H), 7.83 (d, *J* = 8.7 Hz, 1H), 7.42 (d, *J* = 8.3 Hz, 1H), 7.41 (ddd, *J* = 8.5, 7.0, 1.2 Hz, 1H), 7.34 (ddd, *J* = 8.4, 7.0, 1.4 Hz, 1H), 7.24 (d, *J* = 8.6 Hz, 1H), 7.21 (d, *J* = 7.6 Hz, 1H), 6.74 (d, *J* = 7.6 Hz, 1H), 6.68 (d, *J* = 1.5 Hz, 1H), 2.44 (s, 3H), 2.18 (s, 3H); **^{13}C{^{1}H} NMR** (101 MHz, $CDCl_3$): δ 153.5 (C), 143.0 (C), 140.4 (C), 133.4 (C), 132.3 (C), 132.1 (C), 131.4 (CH), 128.7 (CH), 128.0 (CH), 128.0 (CH), 126.2 (CH), 125.7 (CH), 125.1 (CH), 123.3 (C), 122.6 (CH), 93.7 (C), 20.5 (CH_3), 17.2 (CH_3).

The two enantiomers of **6** were separated by semi-preparative chiral HPLC (Lux-Amylose-1, 250 × 10 mm, heptane/isopropanol = 95/5, flow rate = 4.0 mL/min, 200 stacked injections of 100 μL every 2.5 min, and l = 220 nm) t_R = 5.66 min for (*aS*)-**6** and t_R = 6.29 min for (*aR*)-**6**. Using 405 mg of racemic **6** provided (*aS*)-**6** (175 mg, >99% *ee*) and (*aR*)-**6** (178 mg, >99% *ee*) as white solids. The structures and absolute configurations of (*aS*)-**6** and (*aR*)-**6** were confirmed by X-ray diffraction analyses of monocrystals (colorless needles and plates, respectively) obtained by slow evaporation of acetonitrile and dichloromethane, respectively (Figures S4 and S5, Table S4, CCDC 2173777 and 2173778). **Mp** 74 °C (acetonitrile) for (*aS*)-**6** and 78 °C (dichloromethane) for (*aR*)-**6**; **Specific rotation:** (*aS*)-**6** $[\alpha]_D^{25}$ = +29.5 (*c* = 1.0, $CHCl_3$) and (*aR*)-**6** $[\alpha]_D^{25}$ = −29.5 (*c* = 1.0, $CHCl_3$).

Aryne Atropisomer Precursor ***7***. To a solution of (*aS*)-**6** (100 mg, 0.27 mmol, >99% *ee*) in anhydrous dichloromethane (5 mL) was added pyridine (44 μL, 0.54 mmol) at 0 °C. To the resulting mixture was added Tf_2O (90 μL, 0.54 mmol) at this temperature, and the reaction was monitored by TLC until the starting material is no longer detectable (1 h), whereupon a saturated NH_4Cl aqueous solution was added. The resulting mixture was extracted three times with EtOAc. The combined organic layers were dried over anhydrous Na_2SO_4, filtered, and concentrated under reduced pressure. The residue was purified by flash column chromatography on silica gel (pentane/EtOAc = 10:1) to afford (*aS*)-7 (137 mg, 99, 99% *ee*) as a colorless oil. **TLC** (pentane/EtOAc = 8:1) R*f* = 0.69; HRMS (ESI+) *m*/*z*: calcd for $C_{19}H_{18}O_3NSF_3I^+$, $[M + NH_4]^+$ 523.9999; found, 524.0000; **^{1}H NMR** (400 MHz, $CDCl_3$): δ 7.87 (d, *J* = 6.6 Hz, 1H), 7.85 (d, *J* = 6.5 Hz, 1H), 7.45−7.40 (m, 3H), 7.37 (ddd, *J* = 9.1, 7.0, 1.2 Hz, 1H), 7.15 (d, *J* = 7.9 Hz, 1H), 7.15 (d, *J* = 8.1 Hz, 1H), 2.59 (s, 3H), 2.16 (s, 3H); **^{13}C{^{1}H} NMR** (101 MHz, $CDCl_3$): δ 149.3 (C), 146.4 (C), 139.7 (C), 133.5 (C), 132.7 (CH), 132.1 (C), 131.9 (C), 131.9 (C), 130.0 (CH), 128.7 (CH), 128.4 (CH), 128.2 (CH), 126.6 (CH), 125.3 (CH), 125.2 (CH), 118.7 (q, $^1J_{C-F}$ = 319.8 Hz, CF_3), 97.4 (C), 20.5 (CH_3), 18.3 (CH_3); **^{19}F NMR** (376 MHz, $CDCl_3$): δ −71.90; **HPLC** (Lux-Amylose-1, heptane/isopropanol = 95/5, flow rate = 1.0 mL/min, l = 254 nm) t_R = 4.10 min (major), t_R = 4.96 min (minor), 99% *ee*; **specific rotation** $[\alpha]_D^{25}$ = −36.1 (*c* = 1.0, $CHCl_3$).

Cycloadducts ***2a*** *and* ***2b***. In a round bottom flask, the aryne precursor (*aS*)-7 (40 mg, 0.079 mmol, 99% *ee*) was solubilized with 3 mL anhydrous toluene, the toluene was evaporated *in vacuo*, and the flask was placed under an argon atmosphere (drying step). Then, furan (0.57 mL, 7.90 mmol) was added under an argon atmosphere. The resulting suspension was cooled down to −5 °C and trimethylsilylmethylmagnesium chloride (1.0 M in Et_2O, 0.79 mL, 0.79 mmol) was added at this temperature dropwise. After stirring for 16 h at this temperature, water was added to the reaction mixture. The mixture was extracted three times with EtOAc, and the combined organic layers were washed with brine, dried over anhydrous Na_2SO_4, filtered, and concentrated under reduced pressure to afford the crude product. Purification by flash chromatography on silica gel eluted with pentane/EtOAc = 8:1 afforded a 1:1 mixture of the two diastereomers (*aS*)-**2a** and (*aS*)-**2b** (14 mg, 59%) as a colorless oil. The ratio of diastereomers was measured at 1:1 by NMR analyses, and the ratio of enantiomers for each diastereomer was determined by analytical HPLC on a chiral stationary phase with (*aS*)-**2a** having 66% *ee* and (*aS*)-**2b** having 61% *ee*. An analytical sample of (*aS*)-**2b** not contaminated by (*aS*)-**2a** could be obtained to ascertain the attribution of the signals on the HPLC chromatograms. A similar reaction conducted at −20 °C afforded the two diastereomers (*aS*)- **2a** and (*aS*)-**2b** (13 mg, 57%) in 78% *ee* and 76% *ee* respectively. **TLC** (pentane/EtOAc = 8:1) R*f* = 0.49; **HRMS** (ESI+) *m*/*z*: calcd for $C_{22}H_{19}O^+$, $[M + H]^+$ 299.1430; found, 299.1425;

^{1}H NMR (400 MHz, $CDCl_3$, dr = 1:1): δ 7.85 (d, J = 8.2 Hz, 2H), 7.81 (d, J = 8.3 Hz, 2H), 7.50 (d, J = 8.4 Hz, 1H), 7.45 (d, J = 8.4 Hz, 1H), 7.43−7.39 (m, 3H), 7.37 (ddd, J = 8.9, 6.8, 1.2 Hz, 1H), 7.30 (ddd, J = 8.9, 7.0, 1.4 Hz, 1H), 7.11−7.06 (m, 3H), 6.93−6.91 (m, 3H), 6.82 (dd, J = 5.4, 1.7 Hz, 1H), 6.77 (d, J = 6.0 Hz, 1H), 6.75 (d, J = 5.9 Hz, 1H), 5.90 (s, 2H), 5.15 (dd, J = 7.9, 0.9 Hz, 2H), 2.43 (s, 6H), 2.32 (s, 3H), 2.11 (s, 3H); **^{13}C{^{1}H} NMR** (101 MHz, $CDCl_3$, dr = 1:1): δ 148.6 (C), 148.6 (C), 147.5 (C), 147.5 (C), 143.2 (CH), 143.1 (CH), 142.7 (CH), 142.6 (CH), 135.6 (C), 135.5 (C), 133.7 (C), 133.7 (C), 133.2 (C), 132.8 (C), 132.1 (C), 132.1 (C), 129.9 (C), 129.9 (C), 129.0 (C), 128.9 (CH), 128.9 (C), 128.5 (CH), 128.1 (CH), 127.9 (CH), 127.7 (CH), 127.6 (CH), 127.1 (3CH), 127.1 (CH), 126.4 (CH), 126.1 (CH), 126.1 (CH), 125.9 (CH), 125.1 (CH), 125.0 (CH), 81.8 (CH), 81.7 (CH), 81.4 (CH), 81.3 (CH), 21.0 (CH_3), 20.9 (CH_3), 18.2 (CH_3), 18.1 (CH_3); **HPLC** (Lux-Cellulose-3, heptane/ethanol = 80/20, flow rate = 1.0 mL/min, l = 220 nm) t_R = 4.90 min [minor (*aS*)-**2b**], 6.05 min [major (*aS*)-**2b**], 7.44 min [minor (*aS*)-**2a**], 12.13 min [major (*aS*)-**2a**].

Accession Codes

CCDC 2173777−2173778 contain the supplementary crystallographic data for this paper. These data can be obtained free of charge via www.ccdc.cam.ac.uk/data_request/cif, or by emailing data_request@ccdc.cam.ac.uk, or by contacting The Cambridge Crystallographic Data Centre, 12 Union Road, Cambridge CB2 1EZ, UK; fax: +44 1223 336033.

AUTHOR INFORMATION

Corresponding Authors

Yannick Carissan − *Aix Marseille Univ, CNRS, Centrale Marseille, ISM2, Marseille, France;* orcid.org/0000-0002-9876-0272; Email: yannick.carissan@univ-amu.fr

Yoann Coquerel − *Aix Marseille Univ, CNRS, Centrale Marseille, ISM2, Marseille, France;* orcid.org/0000-0003-0646-006X; Email: yoann.coquerel@univ-amu.fr

Authors

Guillaume Dauvergne − *Aix Marseille Univ, CNRS, Centrale Marseille, ISM2, Marseille, France*

Nicolas Vanthuyne − *Aix Marseille Univ, CNRS, Centrale Marseille, ISM2, Marseille, France;* orcid.org/0000-0003-2598-7940

Michel Giorgi − *Aix Marseille Univ, CNRS, Centrale Marseille, FSCM, Marseille, France;* orcid.org/0000-0002-4367-1985

Jean Rodriguez − *Aix Marseille Univ, CNRS, Centrale Marseille, ISM2, Marseille, France*

Notes

The authors declare no competing financial interest.

ACKNOWLEDGMENTS

G.D. thanks the French Ministère de l'Enseignement Supérieur et de la Recherche (MESR) for a Ph.D. fellowship. All authors are grateful to Marion Jean for the measurements of all enantiomeric excesses. Institutional financial support from Aix-Marseille Université (AMU), the Centre National de la Recherche Scientifique (CNRS), and Centrale Marseille are gratefully acknowledged.

REFERENCES

(1) (a) Takikawa, H.; Nishii, A.; Sakai, T.; Suzuki, K. Aryne-Based Strategy in the Total Synthesis of Naturally Occurring Polycyclic Compounds. *Chem. Soc. Rev.* **2018**, *47*, 8030−8056. (b) Pozo, I.; Guitián, E.; Pérez, D.; Peña, D. Synthesis of Nanographenes, Starphenes, and Sterically Congested Polyarenes by Aryne Cyclotrimerization. *Acc. Chem. Res.* **2019**, *52*, 2472−2481. (c) Sarmah, M.; Sharma, A.; Gogoi, P. Exploration of Kobayashi's aryne precursor: a potent reactive platform for the synthesis of polycyclic aromatic hydrocarbons. *Org. Biomol. Chem.* **2021**, *19*, 722−737.

(2) (a) Karadakov, P. B.; Gerratt, J.; Raos, G.; Cooper, D. L.; Raimondi, M. The lowest Singlet and Triplet States of o-Benzyne: Spin-Coupled Interpretation of the Electronic Structure at CAS SCF Equilibrium Geometries. *Isr. J. Chem.* **1993**, *33*, 253. (b) Jiao, H.; Schleyer, P. von R.; Warmuth, B. R.; Houk, K. N.; Beno, R. Theoretical Studies of the Structure, Aromaticity, and Magnetic Properties of *o*-Benzyne. *Angew. Chem., Int. Ed.* **1997**, *36*, 2761. (c) De Proft, F.; von Ragué Schleyer, P. von R.; van Lenthe, J. H.; Stahl, F.; Geerlings, P. Magnetic Properties and Aromaticity of *o*-, *m*-, and *p*-Benzyne. *Chem.—Eur J.* **2002**, *8*, 3402. (d) Poater, J.; Bickelhaupt, F. M.; Solà, M. Didehydrophenanthrenes: Structure, Singlet-Triplet Splitting, and Aromaticity. *J. Phys. Chem. A* **2007**, *111*, 5063. (e) Sánchez-Sanz, G.; Alkorta, I.; Trujillo, C.; Elguero, J. A theoretical NMR study of the structure of benzynes and some of their carbocyclic and heterocyclic analogs. *Tetrahedron* **2012**, *68*, 6548. (f) Kleinpeter, E.; Koch, A. Benzyne—an acetylene- or cumulene-like electronic structure? *Tetrahedron* **2019**, *75*, 4663. (g) Artigas, A.; Hagebaum-Reignier, D.; Carissan, Y.; Coquerel, Y. Multidimensional isotropic magnetic shielding contour maps for the visualization of aromaticity in *ortho*-arynes and their reactions. *Synthesis* **2022**, DOI: 10.1055/a-1867-0674.

(3) (a) Shi, J.; Li, L.; Li, Y. *o*-Silylaryl Triflates: A Journey of Kobayashi Aryne Precursors. *Chem. Rev.* **2021**, *121*, 3892−4044. (b) Fluegel, L. L.; Hoye, T. R. Hexadehydro-Diels−Alder Reaction: Benzyne Generation via Cycloisomerization of Tethered Triynes. *Chem. Rev.* **2021**, *121*, 2413−2444.

(4) Ebel, H. F.; Hoffmann, R. W. Nachweis des Dehydrobenzols in der Gasphase. *Liebigs Ann. Chem.* **1964**, *673*, 1−12.

(5) (a) Berry, R. S.; Clardy, J.; Schafer, M. E. Benzyne. *J. Am. Chem. Soc.* **1964**, *86*, 2738−2739. (b) Schafer, M. E.; Berry, R. S. The Dimerization of Gaseous Benzyne. *J. Am. Chem. Soc.* **1965**, *87*, 4497−4501.

(6) Porter, G.; Steinfeld, J. I. Rate of Dimerisation of Gaseous Benzyne. *J. Chem. Soc. A* **1968**, *1968*, 877−878.

(7) Diau, E. W.-G.; Casanova, J.; Roberts, J. D.; Zewail, A. H. Femtosecond observation of benzyne intermediates in a molecular beam: Bergman rearrangement in the isolated molecule. *Proc. Natl. Acad. Sci. U. S. A.* **2000**, *97*, 1376−1379.

(8) Arora, S.; Hoye, T. R. "Kobayashi Benzynes" as Hexadehydro-Diels−Alder Diynophiles. *Org. Lett.* **2021**, *23*, 3349−3353.

(9) Wei, Y.-L.; Dauvergne, G.; Rodriguez, J.; Coquerel, Y. Enantiospecific Generation and Trapping Reactions of Aryne Atropisomers. *J. Am. Chem. Soc.* **2020**, *142*, 16921−16925.

(10) Kutzelnigg, W.; Klopper, W. Wave functions with terms linear in the interelectronic coordinates to take care of the correlation cusp. I. General theory. *J. Chem. Phys.* **1991**, *94*, 1985−2001.

(11) Lesot, P.; Lafon, O.; Kagan, H. B.; Fan, C.-A. Study of molecular rotational isomerism using deuterium NMR in chiral oriented solvents. *Chem. Commun.* **2006**, 389−391.

(12) Yoshida, S.; Uchida, K.; Hosoya, T. Generation of Arynes Using Trimethylsilylmethyl Grignard Reagent for Activation of *ortho*-Iodoaryl or *ortho*-Sulfinylaryl Triflates. *Chem. Lett.* **2015**, *44*, 691−693.

(13) Frisch, M. J.; Trucks, G. W.; Schlegel, H. B.; Scuseria, G. E.; Robb, M. A.; Cheeseman, J. R.; Scalmani, G.; Barone, V.; Petersson, G. A.; Nakatsuji, H.; Li, X.; Caricato, M.; Marenich, A. V.; Bloino, J.; Janesko, B. G.; Gomperts, R.; Mennucci, B.; Hratchian, H. P.; Ortiz, J. V.; Izmaylov, A. F.; Sonnenberg, J. L.; Williams-Young, D.; Ding, F.; Lipparini, F.; Egidi, F.; Goings, J.; Peng, B.; Petrone, A.; Henderson, T.; Ranasinghe, D.; Zakrzewski, V. G.; Gao, J.; Rega, N.; Zheng, G.; Liang, W.; Hada, M.; Ehara, M.; Toyota, K.; Fukuda, R.; Hasegawa, J.; Ishida, M.; Nakajima, T.; Honda, Y.; Kitao, O.; Nakai, H.; Vreven, T.; Throssell, K.; Montgomery, J. A., Jr.; Peralta, J. E.; Ogliaro, F.; Bearpark, M. J.; Heyd, J. J.; Brothers, E. N.; Kudin, K. N.; Staroverov, V. N.; Keith, T. A.; Kobayashi, R.; Normand, J.; Raghavachari, K.; Rendell, A. P.; Burant, J. C.; Iyengar, S. S.; Tomasi, J.; Cossi, M.; Millam, J. M.; Klene, M.; Adamo, C.; Cammi, R.; Ochterski, J. W.; Martin, R. L.; Morokuma, K.; Farkas, O.; Foresman, J. B.; Fox, D. J. *Gaussian 16*; Revision A.03; Gaussian, Inc.: Wallingford CT, 2016.

(14) (a) Becke, A. D. Density-functional exchange-energy approximation with correct asymptotic behavior. *Phys. Rev. A* **1988**, *38*, 3098−3100. (b) Becke, A. D. Density-functional thermochemistry. III. The role of exact exchange. *J. Chem. Phys.* **1993**, *98*, 5648−5652. (c) Lee, C.; Yang, W.; Parr, R. G. Development of the Colle-Salvetti correlation-energy formula into a functional of the electron density. *Phys. Rev. B: Condens. Matter Mater. Phys.* **1988**, *37*, 785−789.

(15) Zhao, Y.; Truhlar, D. G. The M06 suite of density functionals for main group thermochemistry, thermochemical kinetics, noncovalent interactions, excited states, and transition elements: two new functionals and systematic testing of four M06-class functionals and 12 other functionals. *Theor. Chem. Acc.* **2008**, *120*, 215−241.

(16) Yu, H. S.; He, X.; Li, S. L.; Truhlar, D. G. MN15: A Kohn−Sham global-hybrid exchange−correlation density functional with broad accuracy for multi-reference and single-reference systems and noncovalent interactions. *Chem. Sci.* **2016**, *7*, 5032−5051.

(17) Perdew, J. P.; Burke, K.; Ernzerhof, M. Generalized Gradient Approximation Made Simple. *Phys. Rev. Lett.* **1996**, *77*, 3865−3868 Erratum: ibid.

(18) Tao, J.; Perdew, J. P.; Staroverov, V. N.; Scuseria, G. E. Climbing the Density Functional Ladder: Non-Empirical Meta-Generalized Gradient Approximation Designed for Molecules and Solids. *Phys. Rev. Lett.* **2003**, *91*, 146401.

(19) Perdew, J. P. Density-functional approximation for the correlation energy of the inhomogeneous electron gas. *Phys. Rev. B: Condens. Matter Mater. Phys.* **1986**, *33*, 8822−8824.

(20) (a) Hehre, W. J.; Ditchfield, R.; Pople, J. A. Self-Consistent Molecular Orbital Methods. XII. Further Extensions of Gaussian—Type Basis Sets for Use in Molecular Orbital Studies of Organic Molecules. *J. Chem. Phys.* **1972**, *56*, 2257−2261. (b) Rassolov, V. A.; Pople, J. A.; Ratner, M. A.; Windus, T. L. 6-31G* basis set for atoms K through Zn. *J. Chem. Phys.* **1998**, *109*, 1223−1229.

(21) (a) Dunning, T. H., Jr. Gaussian basis sets for use in correlated molecular calculations. I. The atoms boron through neon and hydrogen. *J. Chem. Phys.* **1989**, *90*, 1007−1023. (b) Woon, D. E.; Dunning, T. H., Jr. Gaussian basis sets for use in correlated molecular calculations. III. The atoms aluminum through argon. *J. Chem. Phys.* **1993**, *98*, 1358−1371.

(22) Weigend, F.; Ahlrichs, R. Balanced basis sets of split valence, triple zeta valence and quadruple zeta valence quality for H to Rn: Design and assessment of accuracy. *Phys. Chem. Chem. Phys.* **2005**, *7*, 3297−3305.

(23) Dolg, M.; Fulde, P.; Stoll, H.; Preuss, H.; Chang, A.; Pitzer, R. M. Formally tetravalent cerium and thorium compounds: a configuration interaction study of cerocene $Ce(C_8H_8)_2$ and thorocene $Th(C_8H_8)_2$ using energy-adjusted quasirelativistic ab initio pseudopotentials. *Chem. Phys.* **1995**, *195*, 71−82.

(24) Scalmani, G.; Frisch, M. J. Continuous surface charge polarizable continuum models of solvation. I. General formalism. *J. Chem. Phys.* **2010**, *132*, 114110.

(25) Marenich, A. V.; Cramer, C. J.; Truhlar, D. G. Universal Solvation Model Based on Solute Electron Density and on a Continuum Model of the Solvent Defined by the Bulk Dielectric Constant and Atomic Surface Tensions. *J. Phys. Chem. B* **2009**, *113*, 6378−6396.

(26) Balasubramani, S. G.; Chen, G. P.; Coriani, S.; Diedenhofen, M.; Frank, M. S.; Franzke, Y. J.; Furche, F.; Grotjahn, R.; Harding, M. E.; Hättig, C.; Hellweg, A.; Helmich-Paris, B.; Holzer, C.; Huniar, U.; Kaupp, M.; Marefat Khah, A.; Karbalaei Khani, S.; Müller, T.; Mack, F.; Nguyen, B. D.; Parker, S. M.; Perlt, E.; Rappoport, D.; Reiter, K.; Roy, S.; Rückert, M.; Schmitz, G.; Sierka, M.; Tapavicza, E.; Tew, D. P.; van Wüllen, C.; Voora, V. K.; Weigend, F.; Wodyński, A.; Yu, J. M. TURBOMOLE: Modular program suite for ab initio quantum-chemical and condensed-matter simulations. *J. Chem. Phys.* **2020**, *152*, 184107.

(27) Grimme, S.; Antony, J.; Ehrlich, S.; Krieg, H. A consistent and accurate ab initio parametrization of density functional dispersion correction (DFT-D) for the 94 elements H-Pu. *J. Chem. Phys.* **2010**, *132*, 154104.

(28) Dolomanov, O. V.; Bourhis, L. J.; Gildea, R. J.; Howard, J. A. K.; Puschmann, H. OLEX2: a complete structure solution, refinement and analysis program. *J. Appl. Crystallogr.* **2009**, *42*, 339−341.

(29) Sheldrick, G. M. SHELXT - Integrated space-group and crystal-structure determination. *Acta Crystallogr., Sect. A: Found. Adv.* **2015**, *71*, 3−8.

(30) Sheldrick, G. M. Crystal structure refinement with SHELXL. *Acta Crystallogr., Sect. C: Cryst. Struct. Commun.* **2015**, *71*, 3−8.